A Search for Tau Neutrino Appearance with IceCube-DeepCore

Michael. J. Larson

January 24, 2018

Contents

List of Figures

List of Tables

1 Introduction

Neutrino Oscillations

2

3 The IceCube Detector

Simulation of the IceCube-DeepCore Detector

4

4.1 Monte Carlo Generators

4.1.1 Background Generation

CORSIKA

The primary background for the observation of atmospheric neutrino events is the other particles present in the cosmic ray interactions in the atmosphere. These interactions produce many particules, most of which are stopped before reaching IceCube by the shielding provided by the Antarctic Glacier. In order to correctly account for the interactions and decays of these particles, the **CORSIKA** generator from the KASCADE Collaboration is used. The CORSIKA generator is a collection of code designed to simulate, interact, and propagate a cosmic ray air shower from the interaction point in the upper atmosphere to the surface. Originally designed for use with surface detectors such as Auger, HAWC, and IceTop, the code has been adapted for use in the IceCube collaboration by identifying the muon (and, sometimes, neutrino) components of the air shower.

CORSIKA has many modes of operation and options for configuration. The standard IceCube simulation of air showers uses the SIBYLL 2.1 hadronization model to follow the interactions through the shower. The low-energy tail of the showering code is handled by a separate hadronization parametrization, but is not relevent for the muon interactions visible in the IceCube detector.

The showers are produced assuming a primary cosmic ray spectrum. Two options are used in IceCube for the simulation of the primary spectrum. The Polygonato model, which throws cosmic rays approximately following the best fit from Hoerandel 20XX. The model requires a selection of a season to simulate due to the annual modulation of the muon flux due to temperature changes in the atmosphere. In typical IceCube simulation, CORSIKA produced using the Polygonato model includes a mixture of muons from all seasons, effectively producing an averaged flux useful under the assumption of equal livetime throughout the year. While this model is out-of-date and not used in recent analyses, it provides a similar shape to newer models until the knee in the cosmic ray spectrum. The natural spectrum of the Polygonato CORSIKA simulation has the benefit of allowing a direct physical interpretation of the resulting spectrum without the need for reweighting and simplifies the prodution of coincident showers, which require a natural spectrum for weighting.

The second model, the five-component mode, reduces the full spectrum of cosmic rays to five effective families: hydrogen, helium, nickel, aluminum, and iron. Each of these components is allowed to have different spectral properties. Elements within each family are assumed to behave similarly. The five-component mode is useful due to the ease with which the user can modify and reweight to different primary spectra, allowing the investigation of different models without the production of dedicated simulation. The simplicity associated with the reweighting of five-component simulation allows IceCube to produce unphysical spectra in order to optimize the production of simulated events necessary for the various analyses. While this slightly complicates the use of the simulation in analyses, the ability to test with

various spectra has been an invaluable tool for high energy analyses, which can be sensitive to changes in the cosmic ray spectrum above the knee. Five-component CORSIKA simulation, due to the unphysical generation spectrum, cannot easily be used for coincident production directly and are currently supplemented by the Polygonato CORSIKA for this purpose.
In both cases, the particles from the air shower are only propagated to the surface of the ice. For analyses using the in-ice array, we take the muons reaching the surface from a CORSIKA simulation and propagate them through the ice, simulating the continuous and stochastic energy losses along the way. The muons are propagated to a surface in the ice consisting of a cylinder with radius 800 meters and length 1600 m centered on the IceCube detector. In order to reach the detector, a muon must result from a cosmic ray interaction of approximately 600 GeV due to the shielding of the glacier. Because of this, CORSIKA simulations typically have a lower energy cutoff of about this value to avoid simulating events that will not reach the detector.
In principle, neutrinos may also be produced using the CORSIKA generator. In practice, this tends to be extremely inefficient for most searches that are no explicitly looking for muons and neutrinos from the same air showers given the extremely low cross section of the neutrino relative to the muon. For this reason, the background generation with CORSIKA in IceCube typically refers to muon events only with no accompanying neutrino.

MuonGun

In many situations, the full CORSIKA generation is unnecessary and wasteful. In situations where the needed muon simulation falls within a relatively narrow phase space, whether that be in energy, angle, or position inside of the detector, it can be beneficial to taylor simulation to the needs of analyzers. Alternatively, there are situations in which the details of the cosmic ray interactions are an unnecessary complication to the final level IceCube analyses. In these situations, IceCube has developed a tool to bypass the full air shower simulation provided by CORSIKA, instead skipping directly to the cylindrical surface inside the ice. This tool, known as **MuonGun**, has the benefit of removing the computationally costly simulation of the full air shower and giving the user more control over the resulting simulated events.
In this generator, the muons are produced on a **generation cylinder** with a radius of 800 meters and length of 1600 meters, matching the final muon positions of the CORSIKA generator. The muons are pulled from a power law spectrum of the user's choice: in this work, an offset power law spectrum is chosen with break at 700 GeV and a range of 160 GeV to 100 TeV. The lower energy range is selected by using CORSIKA simulation to identify the minimum energy required for a muon at this surface to reach and trigger the DeepCore detector.
The angular spectrum of the MuonGun simulation is created by setting a **target cylinder** toward which the generated muon must intersect. For this work, the target is chosen to be the DeepCore fiducial volume, encompassing a cylinder with radius 150 meters and length 500 meters centered on DeepCore at x=(46.3, -34.9, -300).
These features of MuonGun give the generator significant flexibility, allowing for a very focused simulation of muons that would not otherwise be possible with the current implimentation of the CORSIKA generator. The downside, as with all targeted generation, is of course that one must be aware of the limitations. For example, the settings described above will provide a good description of muons reaching and triggering the DeepCore array, but will not include the correct contributions of muons in the outer IceCube detector. This can

result in disagreement between data and simulation if the limitations are not acknowledged and accounted for.
Of course, this abstraction also disassociates the muon at the detector from the air shower, and therefore the cosmic ray, that produced it. In order to properly account for dependence on the cosmic ray spectrum in the muon spectrum, dedicated simulations must be produced using the full CORSIKA generator. By following the interaction, showering, and propagation to the detector, IceCube is able to produce an effective parametrization of the association between a particular cosmic ray spectrum and the muons reaching the detector. This must only be done once, but requires a substantial number of simulated events in order to produce a clean parametrization in position, energy, zenith angle, and variables associated with shower multiplicities higher than one. The version of MuonGun at the time of writing provides the parametrizations for the Hoerandel and H4a cosmic ray spectra. At the time of production for the analyses contained hereafter, all MuonGun simulation is produced assuming a multiplicity of 1, meaning that no bundles are yet produced with this generator. This is a limitation of simulation time: the multiplicity parametrizations vastly extend the parameter space and therefore require significantly more time and effort to handle correctly.

Noise-Only Events

While we only observe neutrinos and muons in the detector, we also observe a significant component of accidental triggers in the DeepCore array. These events, labeled **noise triggers**, arise due to the low trigger threshold. In these events, no actual particle interactions due to muons or neutrinos are observed. Instead, detector noise from various sources coincidentally occur in DeepCore in a way that mimics a very low energy neutrino.
These events are simulated by skipping the generators entirely and allowing the simulation to trigger on the accidental coincidences. Because the events are relatively rare, the simluation requires a special mode, here called **long-frame** simulation, which produces continuous detector readout. Breaking the traditional concept of the "simulated event", these simulation sets instead produce a 100 ms long "event" of random detector noise with the Vuvuzela module. These hits are then run through the simulation of waveforms, coincidences, and triggering as a normal simulated event. After triggering, specialized code, known as **CoincidenceAfterProcessing** is used to divide the long-frame simulation into smaller events more similar to both other simulation as well as actual experimental readout.
Once the events are generated, weighting the events is relatively straightforward: the weight per event depends on the muon interaction rate and the total simulated time. The latter is straightforward to calculate, depending only on the number of long frame simulation events produced and the time window for each of these events. The former is important due to the definition of the noise triggers. These events are, by definition, only able to occur when no muon or neutrino is interacting with the detector. Therefore, the total effective livetime of the simulation must account for the "deadtime" for noise triggers due to particle interactions. This rate, assumed to be approximately 2800 Hz, leads to a change in the effective livetime per event of roughly 15
Noise triggers are particularly computationally expensive to produce, given that they rely on a relatively rare emergent property of random detector noise. In general, a few minutes of effective livetime can take up to two hours to create, with much of the processing time spent on DOMs and hits that do not make it into final triggered events. This limits the total effective livetime that can be simulated in realistic timescales. Current simulations used in this work total approximately two months of effective livetime.

4.1.2 Signal Generation

GENIE

Of course, background simulation is only part of the generation in IceCube. In the end, studies are searching for neutrino candidate events that themselves must be simulated in order to infer properties of the original events. At energies ranging from approximately 1 GeV to 1 TeV, IceCube has adopted the **GENIE** event generator. This code, used widely throughout the oscillation community, includes information about the various interactions, cross sections, and uncertainties involved in neutrino physics from reactor energies upward. Events in the GENIE generator are produced first by selecting events from a pure power law with a given spectral index, often chosen to be either E^{-1} or E^{-2} depending on the purpose. These events are then forced to interact with an electron or nucleon within a specified volume in the ice assuming a constant target density. This is a good assumption, given the small variability in density of the ice due to dust.
The interaction type is determined using the cross section for the given flavor and energy, resulting in a shower of particles. The cross section model, an updated version of GRV98, includes resonant, elastic, quasielastic, and deep inelastic events. The final states are computed using Pythia6, resulting in a final state of particles that is returned to the IceCube software for further processing.
The GENIE code includes tools to reweight events based on uncertainties in eg. the axial masses, cross sections, and various aspects of the interactions themselves. The code is regularly updated, including both new features and retuning of parametrizations to match the latest data. The events produced in this work use GENIE version 2.8.6.

Neutrino-Generator

At energies higher than approximately 100 GeV, there are two changes to the simulation code. At these energies, the contribution to the cross section from deep inelastic interactions becomes dominant while the other interactions become negligible. This allows the simplication of the cross section calculations for no loss in generality. In addition, the cross section continues to rise linearly with the energy. This latter feature requires a detailed simulation of potential interactions far from the detector: namely, the higher energy neutrinos have a non-negligilbe chance of interacting en route to the detector as they pass through the Earth. The **Neutrino-Generator** code (hereafter, **NuGen**) is designed to handle these higher energy interactions. In this model, neutrinos are no longer produced and forced to interact in the ice directly. Instead, a neutrino is produced from a power law spectrum in the atmosphere surrounding the Earth. The event is then propagated through the planet, using the PREM model of the density layers in the Earth to simulate potential interactions en route. Neutrinos which interact may be lost or may be regenerated following the decay of the daughter particles. The energy loss between parent neutrino and surviving daughter neutrinos is recorded in the NuGen files. The daughters are then forced to interact in the detector fiducial volume to give a simulated event.
NuGen can be configured with various Earth models as well as different generation properties. For the studies contained herein, the NuGen files are produced with an E^{-2} spectrum and interact following the CSMS cross section.

4.2 Propagation of the Particles and Light

4.2.1 Modeling with GEANT4

I don't know shit about geant4. Something about how great and wonderous and slow it is at doing particle interactions at low energy.

4.2.2 Lepton Propagation with PROPOSAL

At higher energies, events may be simulated following a parametrization of the energy losses instead of direct simulation of the processes and particles themselves. This parametrization, known as **PROPOSAL**, contains tools to simulate the propagation of leptons and hadrons with ionization, electron pair-production, bremsstrahlung, photonuclear interactions, and decay processes. Each of these is done with a parametrization of the associated energy deposition for a given true particle energy. PROPOSAL may be configured with a minimum energy for the stochastic losses, with all losses below this threshold energy being simulated as continuous, rather than stochastic, losses.

Each of the PROPOSAL parametrizations has its own associated uncertainty ranging between 2% and 10%. For some purposes, these uncertainties are somwhat negligible and result in a linear shifting of the final energy of the events at the detector. This could be accounted for using reweighting techniques, but can generally be handled by a loose normalization uncertainty. For particles with energies below approximately 10 TeV, the additional complication due to the increasingly important ionization losses make the calculation of uncertainties due to propagation non-trivial.

4.2.3 CLSim for Photon Propagation

Once the energy deposition at each position is calculated with GEANT4 or PROPOSAL, the resulting photons must be propagated. There exist two modules which can handle this: Photon Propagation Code **PPC** and OpenCL Simulation Code **CLSim**. The differences are largely of implementation details and both have been verified to give identical results. We will therefore only discuss the latter, CLSim, for the purposes of this document.

CLSim is a code designed to handle the photon propagation in parallelized calculations using an OpenCL device, typically a GPU. The code takes the energy depositions and converts them to photon yields via parametrizations and assumptions about the resulting wavelength spectra of the depositions.

These photons are then propagated through the ice with the current best-fit knowledge about the scattering and absorption properties. Photons continue to scatter until either absorbed or until they reach the face of a PMT in the ice.

At high energies, the light yield is large enough that the propagation of individual photons is both excessively costly as well as unnecessary. In those cases, a feature known as **oversizing** is applied using an oversizing factor typically set to 5. This allows for the production of "weighted photons", which effectively represent bundles of photons with size proportional the square of the oversizing factor. The DOM radius is then increased by the oversizing factor in order to increase the light collection in simulation. With fewer photons to propagate, the simulation proceeds more quickly. The underlying assumptions, that the photon flux is roughly proportional to area and that the flux is high enough that bundles of photons will have similar properties to single photons, is a convenience at high energy when single events may have many photons. This breaks down at low energies, where the photon flux is comparably low and scattering or loss of individual photons matters. Because of the complications associated with oversizing at low energies, most simulations of DeepCore events are done with the oversizing features disabled.

4.2.4 Angular Acceptance and Hole Ice

Once the photons have been propagated to the face of the PMT, an effective angular acceptance is applied. This acceptance, calculated from a combination of lab and in-ice measurements, represents the PMT efficiency as a function of the arrival direction. As expected, the PMT is parametrized to have a negligible efficiency for photons arriving in the downward direction and high efficiency for photons traveling in the upward direction. All other directions follow a curve between these two points. The most forward direction in the PMT, shown with $cos(\eta) = 1$, is thought to be affected by the refrozen ice from deployment. This ice, known as **hole ice**, is believed to have higher concentrations of dust and bubbles, leading to decreased sensitivity for photons arriving from that direction.

There exist three models of the hole ice, two of which utilize the angular acceptance parametrization. The first, known as **H2** gives a model with a scattering length of 50 cm in the bubble column. The 1σ range, represented by the H1 and H3 models, model a bubble column with scattering lengths of 30 cm and 100 cm respectively.

The second, known by the name of the author, **Dima**, is a fit that occurred more recently while simultaneously fitting properties of the ice. This model has been extended with an additional parameter, **p2**, which gives a modification of the most forward region of the PMT. This region is believed to have the most uncertainty, although further studies are ongoing to more directly characterize the most upgoing region.

The last, which exists as part of an updated model of the scattering and absorption in the ice, is labeled **SpiceHD** after the name of the new ice model. This model differs from the previous two in that the hole and bubble column are directly simulated in the ice with no effective angular acceptance curve necessary. In this model, the PMT will have 100% efficiency for any photon reaching the face of the PMT and 0% efficiency for all photons reaching the back of the PMT. This results in a potentially more accurate simulation at the cost of additional processing time and less ease of use for producing systematics sets.

Once the photons have been propagated and the wavelength and angular sensitivity has been applied, the simulation results in a series of **I3MCPE** objects for each DOM. Each I3MCPE represents a single photoelectron worth of charge ejected at the photocathode of the associated PMT.

4.3 Simulating the Detector Electronics

Noise within IceCube-DeepCore

Once the processing of particles and photons has reached the photocathode, detector effects will need to be applied. The first of these, detector noise, is handled by the **Vuvuzela** module in the simulation chain.

Detector noise in IceCube has been studied in depth previously, most notably in my own master's thesis. In brief, studies have shown that there exists a large fraction of the detector noise that displays non-Poissonian behavior in time.

The noise simulation for each DOM is provided by a set of five characteristic parameters, each representing a separate aspect of the assumed process. All five parameters have been previously fit individually for all DOMs using untriggered raw data from the IceCube detector. The simplest of these, the **thermal rate** leads to a standard Poisson process noise model in which all hits are assumed to occur independently with a rate that depends on the temperature of the electronics. The thermal rate appears to fall as the temperature decreases

and is a relatively large component of the noise in IceCube DOMs, with typical rates of approximately 200 Hz.
The next component is another Poisson process, thought to be due to radioactive decays in both the ice and the DOM glass. These noise hits occur at a rate that is independent of temperature with a characteristic rate on the order of 50-100 Hz. Studies of these radioactive components are ongoing, with some evidence that Potassium-40 and Uranium-238 may be responsible for at least some of the observed decays.
Once a decay occurs, there is evidence of a rapid series of pulses occuring in the PMT, leading to a "burst" of noise that can last up to millisecond timescales. These hits are believed to be due to a scintillation or luminescence process related to the glass of both the DOM and PMT. In order to model this bursting behavior, an effective model which represents the timing of consecutive hits from the scintillation process is implimented using a log-normal distribution. This introduces three additional parameters to the noise model: the average number of hits in a "burst", giving the normalization; the mean time between hits within a burst; and the standard deviation of the timing within a burst.
Noise hits in simulation are added to the detector in the form of additional I3MCPEs for each DOM. Once the noise simulation is completed, the combination of I3MCPEs due to particles as well as noise are passed to the next modules.

PMTResponseSimulator and DOMLauncher

The IceCube detector does not directly measure photoelectrons emitted from the photocathode. Instead, the simulated I3MCPEs are converted to **I3MCPulses** within the PMT using the PMTResponseSimulator module. This module, which models the cascading effects within a single PMT, also adds in effects such as the pre-, late-, and after-pulses which are thought to come from defects in the cascading process. The pre-pulses, arriving within a few dozens of nanoseconds prior to the main signal, are thought to arise from the small probability of an electron bypassing one of the dynodes. Late-pulses are likewise thought to be produced by electrons which return to a previous dynode, inducing a signal a few dozens of nanoseconds immediately following the main signal. These signals tend to be small and generally not of importance in the remainder of this document.
After-pulses, which arise from ionization of residual gases in the PMT, are a more significant concern for the purposes of this work. The ionized atoms tend to travel significantly more slowly than electrons, resulting in a delay between the main signal and the subsequent afterpulses that may be as large as 10 microseconds.
The resulting cascade of electrons in the PMT, now including a combination of pulses due to particle interactions, noise, and PMT effects, is detected at the anode as a voltage drop, with the shape of the voltage change referred to as a **waveform**. When the PMT observes more than a threshold voltage drop, typically corresponding to 1/4 of the expected drop from one photoelectron ejected from the photocathode, the DOM begins recording a **I3DOMLaunch**, often referred to simply as a 'launch'.
The waveform of a launching DOM is passed two the two onboard digitizers. The first and more precise of these, the **Analog to Digital Waveform Digitizer**, or **ATWD** will digitize the waveform using 322 bins with 3.3 nanoseconds per bin. Two ATWDs are provided for each DOM, as the digitization process may lead to significant deadtime. In addition, each of the two ATWDs possesses three channels with separate gains. This provides the ability to accurately measure the waveform, even in cases of saturation. The unsaturated ATWD with the highest gain provides a record for the launch.

In addition to the ATWD, there exists a longer-timescale digitizer known as the **Fast Analog-to-Digital Converter**, or **FADC**. The FADC is able to record up to 6.4 microseconds of the waveform in bins of XYZ nanoseconds with no deadtime. This digitizers allows for longer-term behavior to be recorded for the DOM in addition to the detailed information from the ATWD.

As the waveform is being recorded, a signal is sent to nearby DOMs requesting status information. If a nearby DOM, here defined as any of the two nearest above or two nearest below the current DOM, observes a launch within 1 microseconds, then both DOMs are labeled as in **Hard Local Coincidence**, or **HLC**. If no nearby DOM observes a launch within the specfied window, then the launching DOM is referred to as having a **Soft Local Coincidence** or **SLC**.

In the case of HLC launches, the DOM will request the full digitization of the waveforms from both the ATWD and FADC, providing a complete record of the launch. If the launch is instead given the SLC label, the information in the ATWD is dumped and the FADC instead digitizes only the three bins associated with the largest peak of the waveform. While this limits the information available for these launches, the lack of associated nearby launching DOMs provides strong evidence of a launch due to random detector noise.

4.3.1 Event Building

The Simple Majority Trigger

After the DOM has made a decision regarding HLC/SLC status and completed digitizing the waveform, the information is provided to the trigger system. In the actual detector, this occurs at the surface in a system known as the **Joint Event Builder** or **JEB** while in simulation, this is handled by the **Trigger-Sim** module. The JEB system collates information from all DOMs in order to evaluate triggering conditions.

The most common type of trigger used in IceCube analyses is the **Simple Majority Trigger** or **SMT**. This trigger is designed to look for coincidences between DOMs using HLC launches. Each of the SMTs is defined by three fundamental configurations: a DOMSet, which lists the DOMs available for use in the trigger conditions; a threshold number of HLC launches before the trigger fires; and a time window length in which the HLC are required to coexist. In the standard IceCube detector, an SMT using all DOMs with a threshold of 8 HLC launches within 5 microseconds is typically used. This trigger, known as **SMT8** after the number of required hits, is designed for high signal efficiency at energies above 100 GeV with a minimum number of accidental triggers due to random detector noise.

In DeepCore, the desire for lower energy events led to the introduction of a separate trigger, known as **SMT3**. This trigger, using only DOMs within the DeepCore fiducial volume, searches for at least three HLC launches occuring within 2.5 microseconds. This effectively lowers the triggering threshold from roughly 100 GeV with the larger IceCube array to approximately 10 GeV.

Once all triggers are identified, a **global trigger** is defined. This consists of the superset of all triggers occurring within 10 microseconds (?) of one another. All detector readout enclosed within the global trigger as well as additional information within 10 microseconds both before and after the trigger is combined into a single **event**.

4.4 Post-Simulation Processing

4.4.1 Pulse Extraction

From this point in the processing, both data and simulation recieve identical processing. The first step of this processing is to read and extract charge information from the digitized waveforms. This is done using the **wavedeform** module, which accepts and processes the information from the launches in each triggered event. Wavedeform attempts to reconstruct the original I3MCPulses from the digitized waveform information.

Wavedeform uses a parametrized version of the PMT pulse associated with a single photo-electron. Beginning with a single pulse template, a least squares minimization is performed to find the best-fit timing of the pulse to the observed digitized waveform. Additional copies of the pulse template are added and new minimizations are performed until the goodness-of-fit improvement from additional pulses is negligible. The resulting sets of pulses, including associated timing and normalization, are returned with the **I3RecoPulse** class, more commonly referred to as simply **pulses**. These pulses represent the best-fit recreation of the analog pulses in the PMT prior to the digitization process.

Both HLC and SLC waveforms are fit, although the limited information in SLC waveforms necessarily results in the loss of information. When available, information from the ATWD is provided a larger weight relative to the information from the FADC due to the finer binning in time, allowing for more detailed information on PMT behavior near the beginning of the launch of the DOM.

4.4.2 Hit Cleaning

In general, a set of pulses, known as a **pulse series**, contains a significant amount of information due to random detector noise. These additional pulses are not useful for understanding the particle interactions and are therefore typically removed during processing. There exist multiple ways to identify pulses likely to be due to detector noise, three of which will be detailed in order from most strict to most accepting.

LC Cleaning

The most strict cleaning method is also the most straightforward. By selecting only pulses that result from HLC launches, the resulting pulse series can be cleaned of nearly all detector noise. This comes at the expense of a potentially significant amount of information about the event, since all SLC hits are removed.

SeededRT Cleaning

Instead of simply using HLC hits, additional processing may be used to identify potentially interesting SLC hits as well. The **SeededRT** algorithm is one such algorithm, requiring a seed, radius, and time in order to search for additional information in the event. SeededRT begins with a subset of "interesting" pulses, often a selection of the HLC pulses, as a seed. Once a seed is selected, a sphere of the given radius is drawn around each seeded DOM. Any nearby DOMs within the sphere and time window are added to the output pulse series. Once all seed DOMs have been checked, a new seed is created composed of the current output pulse series. The process is then run again, once again updating the output pulse series with any newly discovered pulses. Once no additional interesting DOMs are observed, the final pulse series is written out, able to be used for any subsequent processing.

The most effective set of parameters is dependent on the detector geometry, since a given radius sphere will contain more DOMs in the DeepCore fiducial than the same sphere outside of DeepCore. Because of this, different settings are chosen for these two regions.

Time Window Cleaning

The most general cleaning results in very little loss in pulses due to particle interactions, but allows nearly all noise pulses into the final hit series. This **Static Time Window** cleaning, often referred to using just the acronym **STW** cleaning, looks for pulses near the times associated with triggers. For DeepCore processing, any pulses more than 4 microseconds before or more than 6 microseconds after the SMT3 time are removed.

There exists a second type of time window cleaning applied more rarely. The **Dynamic Time Window** cleaning, hereafter **DTW** cleaning, removes the association with the trigger time. Instead, the window is chosen to maximize the number of hits. DTW cleaning is generally chosen with a significantly tighter window, often consisting of only a few hundred nanoseconds compared to the multiple microseconds used in the STW cleaning.

Time window cleaning is typically used in combination with additional cleaning methods, resulting in little loss in useful signal due to the wide time window (in STW cleaning) or in a very pure set of hits likely to be due to unscattered light.

4.4.3 The DeepCoreFilter

Triggers are generally designed to be as accepting of the proposed physics signal as possible, regardless of the background rates. Typically, limitations exist solely in the processing and storage capabilities in order to prevent the unintentional loss of valuable information. After triggering, various filters may be applied with the sole purpose of removing the collected background. For the purposes of this document, the only filter considered is the **DeepCoreFilter**.

The DeepCoreFilter proceeds by splitting the pulses identified by the SeededRT cleaning into "veto" and "fiducial" pulses, with each DOM given a designation based on it's position in the detector. The average and standard deviation in time are first calculated for the fiducial pulses.

$$
\begin{aligned}
&\bar{t'},\ \sigma_{t'} = 0 \\
&\texttt{For DOM i in } [1 ... \texttt{N}_{\texttt{hits}}] : \\
&\qquad \bar{t'}_i = \bar{t'}_{i-1} + \frac{t_i - \bar{t'}_{i-1}}{i} \\
&\qquad \sigma^2_{t'_i} = \sigma^2_{t'_{i-1}} + (i-1)\frac{\left(t_i - \bar{t'}_{i-1}\right)^2}{i} \\
&\bar{t'} = \bar{t'}_{N_{hits}} \\
&\sigma^2_{t'} = \sigma^2_{t'_{N_{hits}}}
\end{aligned}
\tag{4.1}
$$

All hit DOMs with the first pulse occuring more than one standard deviation away from the mean time are removed from the fiducial pulse series. With the updated fiducial pulse series, a center of gravity, or **CoG**, of the remaining DOMs is calculated.

$$
\vec{x}_{CoG} = \frac{\sum_i^{DOMs} \vec{x}_i}{N_{hits}} \tag{4.2}
$$

An average time is calculated by assuming that all pulses are caused by light emission at the CoG, as would be the case for a cascade-like event.

$$t_{CoG} = \frac{\sum_i^{DOMs} t_i^0 - \frac{\vec{x}_i - \vec{x}_{CoG}}{c_{ice}}}{N_{hits}} \tag{4.3}$$

where t_i^0 denotes the time of the first observed pulse. The standard deviation of this time is then calculated using the fiducial pulses.

$$\sigma^2_{t_{CoG}} = \sum_i^{DOMs} \tag{4.4}$$

Updates to the Noise Simulation 5

5.1 A Summary of Previous Fits

Detector noise is a nuisance in most physics and astronomy experiments. In general, detecor noise for PMTs is assumed to be due to random emission from the photocathode. In this simple model, the noise may be related to the gain and voltage of the PMT, but is independent of external factors. The noise hits appear uniformly in time with a known or measureable average rate following a Poisson process.

This model of the noise was successfully used in the past in IceCube. With the introduction of the lower trigger threshold in DeepCore, however, it quickly became clear that additional sources of noise exist. These additional hits appeared to occur in 'bursts' on a single PMT extending for up to a millisecond. Due to the time-correlations of these hits, the phenomenon was labeled **correlated noise**.

Work done in 2011-2014 **??** showed that the overall noise of the IceCube and DeepCore detectors is well-modeled using a combination of correlated and uncorrelated noise. The empirical model, consisting of a Poisson process for electronic noise and a Poisson process-triggered correlated component modeled with a log-normal distribution, contains five free parameters per DOM fit to each DOM using untriggered raw data from the detector collected over a span of approximately 10 minutes.

The 2014 calibrations were fit DOM-by-DOM by minimizing the chi-squared between the untriggered data and simulation produced with parameters identified using a Metropolis-Hastings algorithm. A distribution of the time between observed hits was used for this fit. Due to the computationally-intensive nature of the fits, the stopping condition was intentionally loosely defined, with a goodness-of-fit of approximately 10% used for most DOMs.

The resulting distributions of the number of hit DOMs and the number of accidental triggers due to detector noise were shown to improve significantly after inclusion of the updated noise model. Analyses at final level reported a significant improvement in fits and a reduction in previously-observed unphysical behavior in fits. The change in the noise model resulted in a change in the rate of neutrinos at final level of up to 50% for a standard oscillation selection in DeepCore and general improvements in agreement between data and simulation rates of other low energy analyses.

5.2 Limitations and Disagreement with Previous Fits

While the rate and shape of the accidental triggers improved significantly compared to past attempts, significant disagreement remained. In particular, the number of triggered events with very few hits (here defined as five or fewer hit DOMs) was shown to still be approximately a factor of two higher in data than in simulation. This region of the parameter space was shown to be dominated by accidental noise triggers in simulation.

The rates of accidental triggers, as an emergent property of the collection of individual PMTs, contains unknown uncertainties due to the individual uncertainties associated with

the noise modeling of each PMT separately. A rescaling of the simulated accidental rates, while difficult to justify a priori without changing the noise rate themselves, proved to be effective in some distributions. In particular, the number of hit DOMs was well-modeled with this approach, resulting in an overall rate agreement of better than 95%.

An evaluation of the limitations of the previous calibration was begun in 2014, uncovering a number of possible improvements.

The original fits were limited due to a number of factors. For example, the fits excluded the effect of atmospheric muons in the detector under the assumption that the approximate hit rate per DOM due to atmospheric muons (approximately 5 Hz) is significantly smaller than the noise hit rate observed in previous calibration (about 600 Hz).

Furthermore, the choice of minimization methods was known to result in potentially-incomplete minimization due to computational limitations. Due to the nature of the fit distributions, there existed significant degeneracy in the parameter space, leading to further difficulties.

In addition, disagreements over the modeling of PMT effects such as afterpulsing led to fits artificially limited to timescales longer than 10 microseconds, allowing the minimizer to only observe part of the correlated noise distribution.

Full waveforms are only recorded from the detector in the case of HLC hits. Because these are rare for noise hits, negligible information was available for fitting at timescales shorter than the FADC readout time of 6.4 microseconds. The noise model itself was used down to 2 microseconds, however, resulting in uncertainty due to the extrapolation of the noise model to shorter times. The limit of 2 microseconds was implemented due to the inherent difficulty in characterizing effects at these timescales due to artificial deadtime related to the HLC launch readout.

5.3 Low-dt Noise from Vuvuzela

In an attempt to address the abitrary limit imposed, a new version of the Vuvuzela code was created with the ability to remove the cutoff. The resulting noise, labeled **low-dt** noise for the short timescales (Δt), was used to produce a simulation of accidental noise triggers for testing without further calibration. These events were used with standard CORSIKA simulation to test the effect of the low-dt noise on low level variable distributions.

The low-dt noise was shown to increase the rate of accidental triggers, leading to better agreement in data and simulation rates. The distribution of the number of locally-coincident DOMs improved, primarily due to the increased rate of accidental triggers.

The distribution of the total charge of events was tested for both HLC hits alone and for all hits. The charge distribution for HLC hits slightly improved. However, the charge expected from simulation and data showed significant disagreements using the low-dt noise when looking at the HLC+SLC hit distribution.

This disagreement implied that the number of SLC hits was increased significantly with the additional low-dt noise. This demonstrated that the noise distribution at very short timescales was an important effect that deserved further attention.

When the noise distribution is extended to shorter timescales, a fraction of the tail of the distribution falls into a single ATWD window of 322 nanoseconds. Furthermore, some fraction of the hits in a burst of correlated noise occur within the three bins read out of the FADC for an SLC hit. With multiple noise hits occuring in such a short time, the DOM will observe a higher voltage in each of the SLC bins. The result is that SLC hits due to noise no

longer occur as single-photoelectron pulses, as is the case when noise hits are rare at the 10 nanosecond timescales, but as an integration of multiple single pulses.

The observation of higher charge in SLC pulses in simulation than data gives one an indication of the extremely short timescale end of the noise timing distribution. Alternatively, the charge distribution of each DOM may therefore be used in the fitting procedure in order to characterize the low-dt end of the noise timing distribution. This provides a direct handle missing from the previous fit, removing some degeneracy that previously existed.

5.4 Updating the Fitting Code

The newly available information provided the potential for improvement in the noise fit distribution as well as a way to remove the abitrary cutoffs used in the previous version of Vuvuzela.

With the opportunity to refit, a number of additional improvements were implemented. In order to include the effect of atmospheric muons, a collection of long-frame CORSIKA was produced. The simulation was halted after photon propagation, giving a collection of muons without detector noise and effects yet applied.

A simulation script was produced to apply the noise, PMT, and DOM simulation for a single DOM using a given set of noise parameters to this long-frame CORSIKA. Information on the timing and charge of the DOM is put into a ROOT file format to ease plotting and fitting. The simulation code was wrapped inside of a calling function, simplifying usage inside of the minimization process.

After the simulation for a given set of parameters, histograms are produced for untriggered data and simulation. As in the previous fits, the time between subsequent hits is used as one of the histograms for calibration of the noise behavior. In addition, the observed charge on the DOM is also histogrammed for use as a second observable.

The range of the histograms, from 6 microseconds until 1 second in the time between hit and 0-5 photoelectrons per DOM launch, provides sensitivity to the full range of the noise distribution.

Using the two distributions, a Poisson binned likelihood is formed using the standard equations. In this case, with the simulation in bin i of histogram j denoted by f_{ji} and the data hits in the same bin denoted by d_{ji} and ignoring normalization constants, the log-likelihood takes the form

$$LLH = \sum_{j} \sum_{i}^{\texttt{nbins}_j} d_{ji}\text{Log}(f_{ji}) + f_{ji} \tag{5.1}$$

For more information on the derivation of the likelihood, see **??**. The negative log-likelihood, $-LLH$ is minimized as a function of the five noise parameters using the iMinuit, a python wrapper for the minuit2 package.

Initial fits showed a lack of constraining power from high charges in the charge distribution. To provide more weight to high charges, the histogram of the charges was weighted by the value of the observed charge. This reduces the weight of very low charge launches, but increases the weight of higher charges.

Additional work showed that the charge distributions between data and simulation demonstrated significant disagreement. A scale factor applied to the charge in simulation was introduced as a free parameter in the fit to account for this. To limit the computational complexity of the added parameter, the minimization over this charge scale factor is done as

a separate step in the calculation. This assumes that the difference is a calibration issue in the data rather than a simulation problem. This, in fact, has been shown to be the case, with an updated charge calibration now applied to data at final level. Further information on the charge disagreement between data and simulation can be found in section **??**.

The previous calibration attempts explicitly avoided fitting the behavior below 10 microseconds due to the potential for mismodeled PMT effects. In particular, it was noted that mismodeled afterpulsing behavior could lead to pulls in the noise parameters. The default value in simulation, assumed to be 5.6% for all PMTs, failed to take into account variations in the effects on each individual DOM. In the updated fit, the afterpulsing behavior has been investigated for each PMT by including an overall scale factor on the afterpulsing probability.

Late pulses, produced by electrons which backscatter to previous dynodes during the multiplication process, were also investigated for their effect on the goodness-of-fit in the noise distributions. These pulses occur at timescales of 50-200 nanoseconds and therefore are outside of both the SLC charge and timing distribution window. Regardless, the late pulsing behavior was found to have a small impact due to both the rarity of late pulses as well as the lack of detailed information to constrain the distribution.

The effect of the afterpulsing parameter allowed some fits to fall into a poor local minimum. In those cases, the interplay between the parameters led to a fit that could no longer produce a reasonable fit. In these cases, the probability of observing an afterpulse following a photoelectron would be moved from 5.6% to the unrealistically high value of 20%. This would, in turn, force the mean value for the log-normal timing distribution to move toward higher values and the sigma value to become unrealistically large.

These fits were noticeable when looking at the best fit value of the afterpulsing probability, with a distinct population appearing due to this behavior. In order to constrain the fit to more realistic values, bounds were added to both the log-normal mean and afterpulsing probability.

Due to the computational power required to produce large amounts of effective livetime, a tiered approach was employed in the calibration process. Initial fits were seeded with the previous noise parameter fit values obtained in 2014. For these events, a course binning and short effective livetime of just one minute were used. In addition, a weak tolerance value was used, allowing the minimizer to quickly migrate to the neighborhood of the global minimum.

When the first tier completes the minimization process, the fit is begun anew with more effective livetime, more bins, and a stronger tolerance. The second tier used a 5 minute effective livetime.

The third and final tier increased the effective livetime to 10 minutes and again increased the number of bins.

5.5 Results of New Noise Fits

New calibration fits were completed over the course of approximately two months for nearly all DOMs in the IceCube detector. String 21 was absent from the updated untriggered data and was therefore left unfit.

The noise fits were checked for correlations between parameters after convergence. One immediately notable feature is the number of DOMs with afterpulsing at the fitter boundary. The likelihood values associated with these fits, however, appear to be consistent with other fits. Due to a planned overhaul of the afterpulsing simulation, the fit values of the

afterpulsing probabilities have not been adopted for simulation. Therefore, no further investigation of the probabilities has been persued.

Some of the noise parameters have expected behavior. In particular, there exists a Poisson process component of the noise model that is assumed to be associated with the electronic noise, which should show increasing rate with increasing depth due to the rising temperature. This effect, though weak, is apparent after the fitting procedure.

Other parameters should be independent of depth. As a test of the fits, each of the other parameters is plotted as a function of depth as well. No significant correlation is observed.

Finally, the likelihood itself should be independent of depth. This final test shows surprising results in at least two ways: a 'band' structure appears in the plot. and there appears to be a depth-dependent decrease in the likelihood value, indicating that the lower part of the detector yields better fit results. This was initially unexpected, given that the noise is an internal property of the DOM and not of the surrounding medium.

This effect occurs due to a combination of factors. It is worth noting that the fits are not independent of external factors. Indeed, the fits themselves use the long-frame CORSIKA to model the effects of muons in the untriggered data from the detector.

This leads to two subtle limitations in the fitting process. The long-frame CORSIKA is produced with a single flux model, in this case the model of Hoerandel. Because the long-frame CORSIKA cannot be reweighted to other models, uncertainties or mismodeling in the muon flux can lead to disagreement in the fitting of noise parameters. The muon flux decreases with increasing depth, resulting in a lower muon contamination, and consequently smaller effects from mismodeling of the muon background, for deeper DOMs.

In addition, the long-frame CORSIKA implicitly assumes a single model of the ice for photon propagation. Mismodeling of the scattering and absorption of the ice therefore may also give rise to disagreement in the noise calibration process. While large-scale properties of the ice are believed to be well-reproduced by the chosen ice model, SpiceLea, there will inevitably be remaining disagreements.

The net effect of these two assumptions in the muon simulation is effectively correlated with the convolution of the ice model and the muon flux. In particular, the best fits occur where the DOM is either A) well-shielded from light due to muons by the large depth or B) well-shielded due to large absorption in the ice. In both cases, the contamination from light due to muons in the fitted time and charge distributions will be small, leading to a more 'pure' noise distribution that is well-fit by the assumed model.

The sensitivity of the noise calibration procedure to underlying physics of both the muon flux and the absorption properties in the detector imply that little further improvement is likely without work on one or both issues. Simulation of long-frame CORSIKA is, unfortunately, unlikely to be updated to a newer flux model in the near-term due to technical limitations. As the primary uncertainty affecting the goodness-of-fit appears to be due to the visibility and flux of the muons themselves, merely updating to a newer model of the ice will be unlikely to significantly improve the current fit parameters.

The newly calibrated low-dt Vuvuzela was provided to the IceCube simulation group in January of 2015 and quickly integrated into the low-energy simulation chain. New neutrino, muon, and accidental noise trigger simulations were produced soon thereafter. The updated noise model shows significantly better agreement in both the total charge distribution and the number of hit DOMs for both HLC and SLC+HLC hits. The rate of accidental triggers improved relative to previous calibrations, with the remaining rate disagreement reduced

from 50% to approximately 15%. Negligible effect was observed in the low-energy neutrino events at final level for existing samples.

Low-Energy Muon Simulation

6

6.1 Long-Frame CORSIKA for DeepCore

One of the primary difficulties for low energy analyses in IceCube is the modeling of backgrounds. Two significant backgrounds exist for a standard muon neutrino disappearance measurement: the events due to cosmic-ray induced muons and the events from accidental triggers in the detector due to random detector noise.

The two types of simulation are somewhat interdependent. In particular, the accidental trigger rate, defined to include only events in a trigger is primarily caused by noise hits, relies on the rate of atmospheric muons to calculate an effective livetime for possible noise triggering. In turn, the atmospheric muon triggering and filtering rate depends somewhat on the characteristics of the noise model used in the simulation.

At the lowest energies, the interplay between atmospheric muons and noise becomes more muddled. The falling muon spectrum ensures that there are a significant number of muons that potentially reach the IceCube detector even down to cosmic ray primary energies of approximately 600 GeV, where the overburden from the glacial ice yields a natural cutoff to the specrum. At these energies, a shift in either the muon rate or the noise rate can change the hit rates at the top of the detector. These low-brightness muons are largely indistinguishable from noise hits, but are not simulated using the Vuvuzela module. Ignoring these muons can result in a systematic mismodeling of the detector background that changes as a function of depth, with the worst agreement at the top of IceCube. These muons, called **sub-threshold muons**, have been shown to be responsible for a significant fraction of hits in the detector [**heereman_thesis**].

While the 5-component CORSIKA described in 4.1.1 generally gives much more freedom to fit and correct for spectral characteristics, the events cannot easily produce the low-energy muon background characteristics at the top of the detector. Instead, the most accurate way to model these effects relies on long-frame simulation described in 4.1.1. These frames, consisting of a continuous detector simulation over the course of tens of milliseconds or longer, can be combined with CORSIKA simulation in order to produce the most accurate background simulation possible with current tools.

Long-frame CORSIKA generally requires a modeling of a natural flux of events in the detector. Given the currently available toolset, only the polygonato mode of the CORSIKA generator is therefore able to be used for long-frame generation. While there are currently ideas for how to generate with a more acccurate spectral model, they prove to be inefficient without a reparametrization of the generation from the CORSIKA code itself and will not be discussed here.

To produce long-frame CORSIKA simulation, a few modifications of the standard simulation scheme are required. A frame length, τ is chosen at the start of simulation. Longer values of τ will generally yield more accurate simulation due to issues at the start and end of a frame, although this is a minor concern in practice. With this time, an expected number of particles may be extracted given a spectrum Φ_μ and a simulation volume V:

$$\bar{N_\mu} = \int_{t=0}^{\tau} \int_E \int_\Omega \int_V \Phi_\mu \tag{6.1}$$

This is an analytic formula, yielding the poissonian expectation on the expected number of muons in the simulation volume. A number of muons is then calculated as a poisson-fluctuation of this number. The CORSIKA generator will produce the requested number of muons in this time frame. These muons can be either single muons or occur as muon bundles. In the latter case, the entire bundle is treated as a 'muon' for the purposes of this section.

The muons are evenly distributed throughout the simulation window following the assumption that each muon is independent of all others (ie, that they are not due to the same cosmic ray interaction in the atmosphere). From this point, the long-frame simulation scheme described in 4.1.1 continues, with detector simulation and splitting occuring in the CoincidenceAfterProcessing module.

Long-frame CORSIKA simulation is a useful tool for low energy analyses, yielding a collection of accidental trigger events and muons that would otherwise be produced separately and require reweighting. In addition, emergent properties of the subthreshold muons are included in these simulation sets. Unfortunately, the production of long-frame CORSIKA simulation is particularly computationally expensive and of limited use for most higher energy analyses ongoing in the IceCube collaboration. Very little long-frame CORSIKA simulation is therefore available.

For this work, long-frame CORSIKA simulation was crated with an effective livetime of approximately two weeks. Such a sample required months of simulation time, severely limiting the potential usefulness for analyses. Still, the existing sets proved useful and necessary for the work in 4.4.3. Furthermore, the sets provided the first background estimates for both accidental triggers and atmospheric muons for the PINGU/Phase 1 detector described in 8.8.4.

Initial tests with the long-frame CORSIKA simulation showed, for the first time, notable disagreement in the charge distributions in data and simulation described further in 5.1.

6.2 MuonGun for DeepCore

6.3 Simulation Efficiency with KDE Filtering

The production of background atmospheric muons is the most computationally expensive part of oscillation analyses in IceCube. For the primary analysis of this thesis, full CORSIKA simulations have proven to be impractical. When simulating at the detector threshold, many of the produced showers lead to no significant contribution to the detector output, leading to significant inefficiency. In addition, the choice of cuts employed (see 6.3) lead to a low simulation efficiency at final level that has both strong energy and zenith dependences.

For this work, a set of 3×10^9 muons were produced using collaboration resources over a period of approximately three months. Muons were produced following the MuonGun scheme described in 4.1.1, with all muons aimed toward the DeepCore fiducial volume. The resulting generation-level distributions are shown in **??**. The muons follow the offset power law described in 4.1.1 in energy and the expected zenith angle spectrum from the underlying flux model of [**h4a**]. The generated muons show azimuthal symmetry as expected.

After processing to the final level of the GRECO event selection (see 6.3, the background muon simulation retains approximately 9000 simulated events of the original sample. This remaining subsample may be used to estimate the simulation efficiency of muons in this selection. The efficiency is most easily observed with low energy muons that travel very

downgoing, as seen in ??. These events make up the majority of simulated muons at generation level, but no such events reach the final level of the analysis.

In addition to the energy- and zenith-dependent effects, the GRECO selection exhibits strong azimuthal selection bias. This arises due to two main effects. The first is the offset between the center of IceCube (and therefore the center of the generation volume) at $(x, y, z) = (0, 0, 0)$ and DeepCore at $(x, y, z) = (XXXXXXX)$. This gives rise to an azimuthal effect appearing as a sinusoidal variation of the minimum generated energy of events at final level.

The second is the regular hexagonal structure of the IceCube volume, with long "corridors" through which muons may reach DeepCore without crossing any strings. Cuts designed to look for hits left in the veto region produce these azimuthal biases when muons close to strings (ie, outside of the "corridors") are more likely to be identified and removed than those further from strings (inside of the "corridors").

In order to improve simulation statistics at final level, the existing MuonGun simulation scheme was modified to include an energy-, zenith-, and azimuthally-dependent prescale factor. This approach, here entitled **KDE Filtering**, allows simulation to be produced with a known bias matching that of a given set of input files.

In this scheme, the **kernal density estimator** (**KDE**) from SciPy [**scipy**] is applied to all remaining events at final level of the GRECO event selection. The KDE uses a Gaussian kernal to represent each event in energy, zenith, and azimuth. The resulting KDE is normalized to produce an approximation of the final selection probability density function.

In the new simulation scheme, an event is produced using standard settings for MuonGun generation. Immediately following generation, the probability of the new event reaching final level is calculated from the KDE, with typical values of approximately 10^{-4} for a likely event and 10^{-9} or lower for unlikely events. A prescale multiplicative factor of 10^5 is used to set the overall probability scale. The product, p of the prescale factor and KDE-derived probability may not exceed 100% and any values for which this may be the case are directly set to 100%.

Using a random number generator, this p factor is used to retain or reject the muon event. The simulation then proceeds as normal, with photon propagation, detector simulation, triggering, and filtering.

When events need to be weighted by a flux model, the p factor must be included as well. The modification to the weighting scheme requires the use of the original MuonGun weighting code in the usual scheme. The total weight is then scaled by $\frac{1}{7}p$, which corrects the rates and uncertainties for the simulated events.

By removing unlikely events early in the simulation chain, the required computational resources are significantly reduced. In addition, the updated simulation scheme gives the opportunity, for the first time, to study various detector systematics affecting the atmospheric muons at the final level of oscillation analyses.

By way of comparison, the total amount of time required to produce 9000 events at final level of the GRECO selection with similar available resources reduces from three months under the standard scheme to approximately four days using the KDE filtering method.

7 GRECO: An Event Selection at the Limits of DeepCore

7.1 Low-En Level 3 Cuts

7.1.1 GRECO Level 4 Cuts

The first GRECO-specific cut level, designated **level 4**, or **L4**, was first introduced in 2011 using variables common to higher energy cascade analyses within IceCube.

At the start of this series of cuts is requirement of at least three hit DOMs in the hit series associated with an event. This is an extremely loose cut, required solely for the successful processing of other cuts.

The remaining cuts at L4 can be divided into two groups: those that rely on a rough reconstruction of the event and those that are based solely on charge deposition.

FirstHit Z

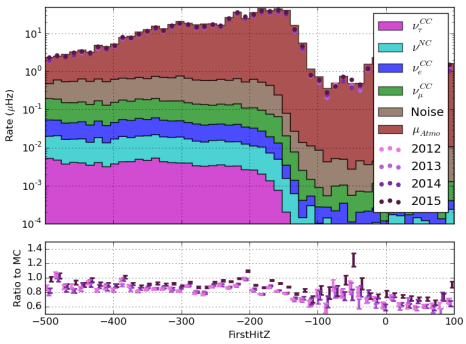

Figure 7.1 – The Z position of the first hit in a cleaned hit series. Note the shape difference between the atmospheric muons in red and the various neutrino flavors, particularly above -200 meters.

Muons generated in the upper atmosphere through cosmic ray air showers will generally be visible as they enter the detector. As they pass through the veto layers, the muons may emit light via Cherenkov emission or via stochastic processes. This light leaves a signature behind in the detector in the form of hits along the true muon track.

Because the muon tracks are primarily steeply inclined, most will leave hits in the upper part of the detector. Neutrinos, on the other hand, will emit light following an interaction. For the low-energy neutrinos of interest to this analysis, interactions will occur primarily in the DeepCore fiducial region, leading to little or no light emission in the top half of the detector. This difference between neutrino and muon emission in the upper part of the detector can be used to identify background muons with little additional processing. For this analysis, the first hit in a cleaned hit series, the time-window cleaned DeepCore pulses, is called the **FirstHit Z** in the Level 4 cuts.

NAbove200

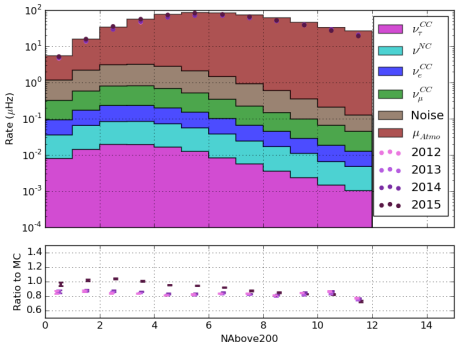

Figure 7.2 – The number of hits above Z=-200 meters

The position of the first hit in DeepCore is not the only low-level cut to arise from the emissions of the muon and neutrinos. The total charge of recorded hits occuring in the top of the detector is also used in the analysis. This variable, known as **NAbove200**, counts the amount of charge occuring before the SMT3 trigger above a depth of -200 meters.

QR6/C2QR6

After a particle interacts, the light emission as a function of time will depend on the type of particle emitting. A very basic model of cascade-like events assumes that photons are emitted roughly instantaneously from a point-like source at the interaction vertex. The photons then travel outward according to a random walk with absorption, leading to a decay in the observed number of photons over time. A muon, however, acts as an extended source and will emit at multiple points along the muon track until it either falls below the Cherenkov threshold or is stopped.
The light emission is, therefore, more likely to be "peaked" in time for neutrinos than for muons. Using this information, two variables are designed to seach for this peakedness in the light detection over time.
The first of these, the **charge-ratio within 600 ns** (hereafter **QR6**), is the ratio of the charge occuring within 600 ns of the first hit compared to the total charge of the event. The value of 600 ns was chosen in a previous analysis and is not re-optimized here. Regardless, this time corresponds to roughly two ATWD time windows or approximately 180 meters at the speed

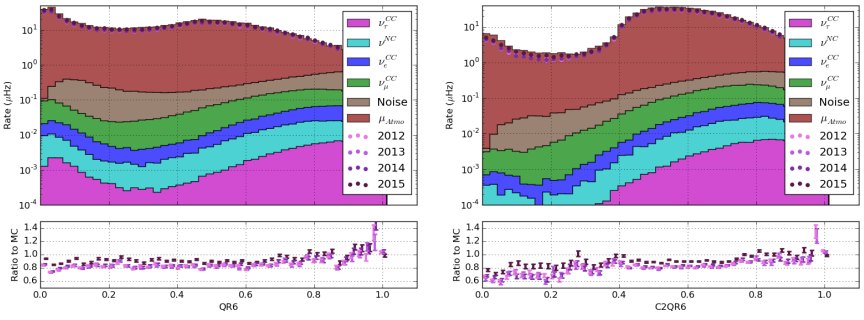

h

(a) QR6 **(b)** C2QR6

Figure 7.3 – The charge ratio variables used in the L4 cuts.

of light in vacuum. This distance, which will correspond to a wide swath of the DeepCore fiducial volume, provides some separation between muons and neutrinos.

QR6 plot

Neutrinos and muons do not produce the only hits observed in the detector, however. Random detector noise, in particular, can significantly change the choice of time used. In order to check the effect of random noise contributing the first few hits of the event, a second variable, known as **C2QR6**, is introduced. This variable is calculated in an identical way to QR6, but the first two observed hits are ignored.

C2QR6 plot

Tensor of Inertia

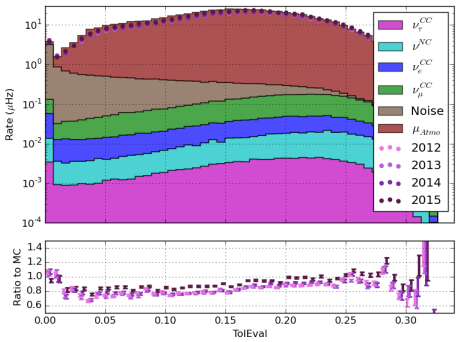

Figure 7.4 – The eigenvalue ratio from a ToI calculation. Larger values indicate more apparent elongation in the event.

At this early level, the shape difference in the observed hit pattern will be relatively clear. Neutrinos with energies in the range of 1-100 GeV will appear to be rather small and compact, while muons will have a longer extent in one direction along the muon track than perpendicular to it. In order to utilize the shape differences between these two types of particles, the **Tensor of Inertia eigenvalue ratio** (more briefly, **ToI**) is used. This variable is defined in a similar way to the tensor of inertia from mechanics, with the measured charge taking the place of the mass.

$$I_X = \sum_{i=0}^{nhits} (y_i^2 + z_i^2) q_i I_Y = \sum_{i=0}^{nhits} (x_i^2 + z_i^2) q_i I_Z = \sum_{i=0}^{nhits} (x_i^2 + y_i^2) q_i \tag{7.1}$$

These three moments yield information about the shape of the event. The eigenvalue ratio is defined as

$$e = \frac{\texttt{max}_j(I_j)}{I_x + I_y + I_z} \tag{7.2}$$

Improved Linefit Speed

The L4 BDT

A Boosted Decision Tree (**BDT**) is trained at L4 to further reduce the atmospheric muon background by a factor of 10x.

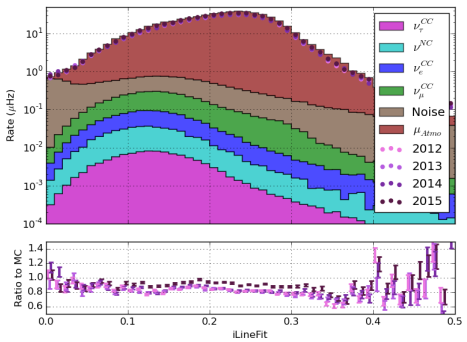

Figure 7.5 – The apparent speed, in units of meters per nanosecond, corresponding to the hits in the event. Faster speeds are associated with particle travel instead of light travel.

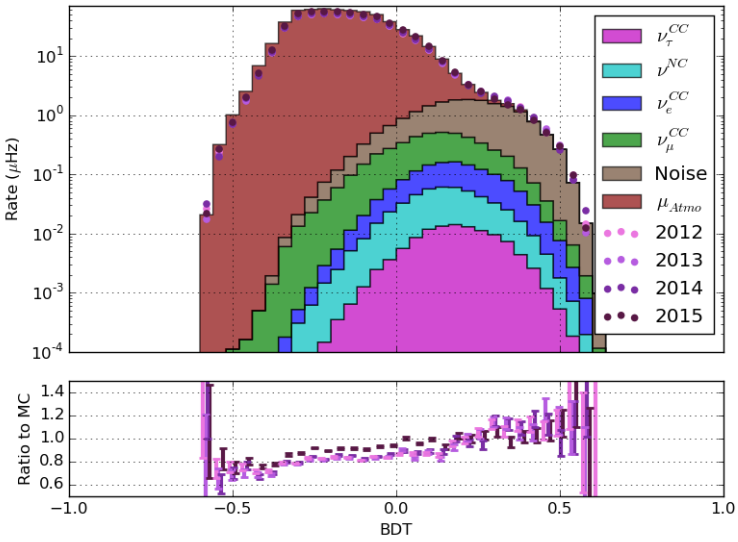

Figure 7.6 – The distribution of the boosted decision tree used at L4. A cut is applied at 0.04 to remove a significant fraction of atmospheric muon background events. Note the ratio, which shows disagreement in the very muon-like region. The region of disagreement is removed by the cut.

The variables described above were provided to a BDT training using the CORSIKA 7437 and IceSim3 GENIE simulation.

Burn sample distributions match in the years 2012/3/4/5, but are notably different for 2011. I believe the reason is related to the deployment: once new DOMs are deployed, they take 1-2 years to completely cool down 2011 is therefore excluded for this analysis.

Comparisons to MC show mild disagreement, particularly in the most muon-like regions that get cut away. Its not obvious what is the cause of the disagreement, although its possible that the assumed cosmic ray flux model (H4a) is simply an inaccurate model of some part of the spectrum that contributes. This may be particularly true, since H3a and H4a contain different compositions at high energies. These differences would contribute to different parts of the atmospheric muon spectrum at the detector, where the highest energy atmospheric interactions leading to visible muons will occur at the horizon. If these (or other systematics on the CR/muon spectra) give rise to different HE muon distributions, those muons would appear to have clear tracks and would show up on the far left of the BDT distribution.

In the right side of the plot, a shoulder attributable to the noise triggers is visible. While this is initially surprising, the reason for this is obvious: the BDT was originally trained with CORSIKA set 7437 and weighted GENIE sets. Both cases had incorrect modeling of the detector. Both had DOM oversizing applied and DOM efficiency set to 0.9 (the old nominal value) instead of the 0.99 that we now use. The training itself lacked any pure noise triggers as a reference, and so the BDT picked the most obvious feature of the GENIE sets: that the signal events were primarily low energy with lower light deposition than the background. These are also key features of the noise triggers.

7.1.2 GRECO Level 5 Cuts

The next stage of cuts, know as the **GRECO Level 5**, or more simply, **L5**, is structured in a similar manner. Once again, there exists both a relatively simple cut dedicated to removing accidental triggers due to noise as well as a BDT consisting of six variables.

L5 Straight Cuts

The former is a again cut on the number of hits similar to the cleaning applied in the L3 cuts. This time, however, a slightly different cleaning is applied, consisting of both a static and a dynamic time window applied to the split DeepCore pulses. The static window, with a width of 7500 nanoseconds, removes hits that are far from the trigger in order to limit the effect of random detector noise. The dynamic time window is designed to specifically look for a set of hits spaced very closely in time. For the L5 noise trigger cut, a dynamic window is chosen of 200 nanoseconds.

After the two time window cleaning algorithms are applied, the resulting hit series is required to posses at least 3 remaining hits to be accepted for further processing.

Time to 75% Charge

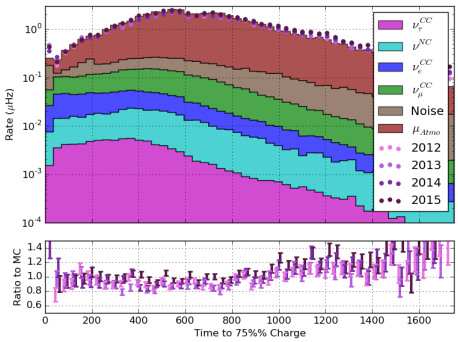

Figure 7.7 – The time to accumulate 75% of the total charge of the event.

The first variable used to create the L5 BDT is the amount of time to accumulate 75% of the total charge, the t_{75}. The idea behind this variable is again similar to that of the QR6 and C2QR6 variables and will not be repeated here. However, the variable is now produced in the reverse manner: where the QR6 variable refers to the amount of a charge in a given window, the t_{75} instead attempts to find the amount of time for a given charge level, providing an additional handle on the total event length and timing distribution.

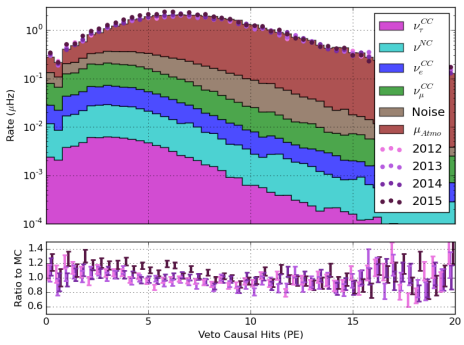

Figure 7.8 – The amount of causally-connected charge discovered in the veto region.

Veto Identified Causal Hits

The **Veto Identified Causal Hits** (**VICH**) algorithm is a second choise for the L5 cuts that relies solely on low-level charge information. In this case, we improve on causality constraints using the trigger time and the position of the first DOM to contribute to the trigger. The time and distance are calculated to each other hit relative to this simplistic event vertex. Any hits that occur in a window before the trigger that are approximately causally connected to this hit are recorded, with the total charge thus recorded giving the cut variable. The window is described in **??**

First Hit ρ

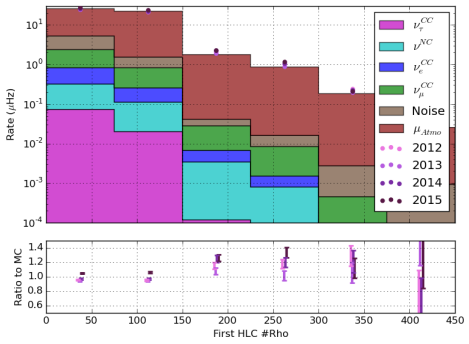

Figure 7.9 – The radial position of the earliest hit of a cleaned hit series. The radial position is measured relative to string 36, the center of DeepCore.

Further simple event vertices give additional separation power. In particular, the radial position of the first hit in a STW cleaned (7500 ns) hit series encompassing solely the DeepCore fiducial volume may be used to identify incoming atmospheric muon events.

Quartiles CoG

The traveling distance of a muon may be exploited in order to identify muons as well. In particular, a track-like event is expected to travel over a longer distance than a cascade-like event of a similar energy. Looking at the first and last quartiles in charge, the length of the vector from one of the CoGs to the other can give some simple indiciation of the length of a hypothetical track in the event.

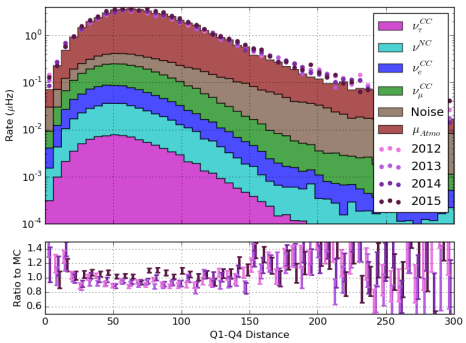

Figure 7.10 – The distance between the centers of gravity of the first and last quartile in time.

Z-Travel

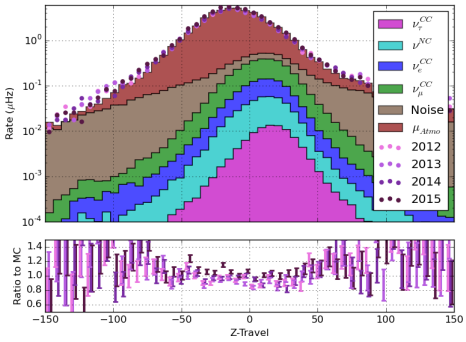

Figure 7.11 – The distance traveled in Z between the first and last quartile of hits in time.

Atmospheric muons are primarily a downgoing feature of the detector, with a flux that approaches zero at the horizon. Muons will, therefore, leave some information in the depth and directional information collected by the detector. The first variable to utilize this, **Z-Travel**, identifies the distance in the z-direction between the first and the last quartile of hits using the CoGs calculated in the previous variable.

SPE Zenith

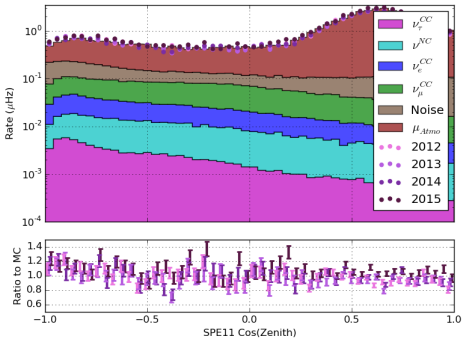

Figure 7.12 – The zenith angle distribution of events from an 11-iteration SPE fit. The fit assumes an infinite track hypothesis and uses only hit DOMs.

More advanced reconstructions are viable at this level, providing new potential for the identification of atmospheric muons from neutrino candidates. Using the first pulse on each DOM, a likelihood reconstruction may be produced. A fast likelihood reconstruction assuming an infinite track passing through the detector with light scattered via the Pandel scattering model of ice is one such tool.

The Pandel model of scattering, while known to be inaccurate, provides an analytic form that is fast to evaluate in order to find the charge expectation as a function of relative position and direction between the hypthesized track and each DOM. The reconstruction is begins with a seed of some description that my slightly gin-addled mind with no internet access cannot recall. A total of eleven directions are used as seeds around the seeded position and time, including a seeded direction. For each hypothesis, the expected charge at different time steps is compared to the observed charge at each DOM using a Poisson binned likelihood. The best-fit of the eleven reconstructions is returned.

Again, atmospheric muons are primarily downgoing events. Therefore the direction of the reconstructed track is a useful tool for separating neutrino signal and atmospheric muon background.

The L5 BDT

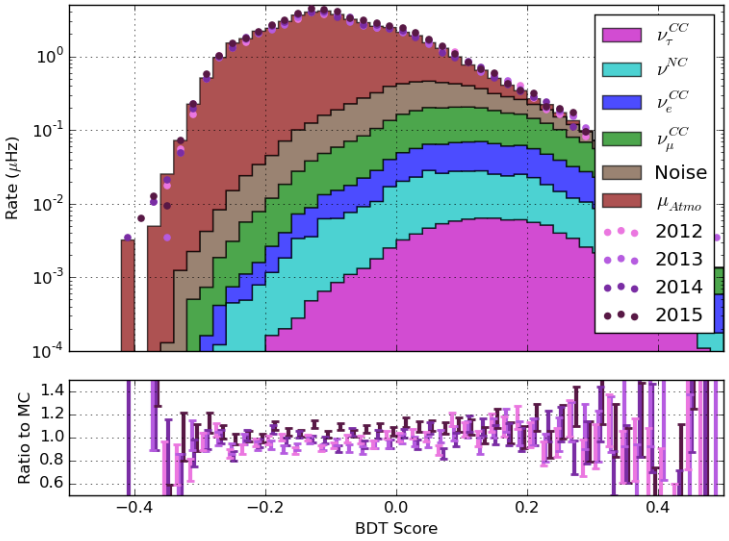

Figure 7.13 – The distribution of the boosted decision tree used at L5. A cut is again applied at 0.04 to remove a significant fraction of atmospheric muon background events.

The six variables described in this section are again used to create a BDT. At the time of training, updated versions of both the GENIE and CORSIKA simulations were provided as part of a ongoing upgrade of the IceCube simulation. In particular, the L5 BDT was trained using simulation files containing the then-newly available Vuvuzela noise model and an updated version of the GENIE Monte Carlo generator.

A set of fifteen variables were tested. At each step of the training, the least important variable was removed to limit the possible effects of overtraining. The process continued until changes in the cut efficiency larger than 1% were observed, resulting in a boost decision tree containing the six most important variables tested as described above.

The distribution of BDT score is shown in ??. The data and simulation show good agreement across the range of scores. In addition, the distribution of shows some separation from the neutrino events, providing some cut power.

A cut is placed at a score of 0.04, which gives approximately 95% background rejection with a somewhat significant hit of 30% to all neutrino rates.

7.1.3 GRECO Level 6 Cuts

Unlike previous levels, the GRECO L6 does not rely on a trained boosted decision tree. The choice was made to use solely stright cuts due to initial concerns about the significantly limited background simulation. Such a limitation could lead to overtraining, a situation difficult to test with so few simulated events.

Instead, there are effectively two types of cuts used in the GRECO L6: those that deal, directory or indirectly, with removing accidental triggers and those that focus on the starting containment of events in the DeepCore fiducial volume.

Fill-Ratio at L6

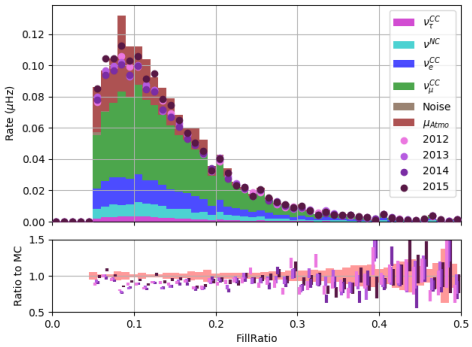

Figure 7.14 – The fill-ratio distribution. Note the excess of noise triggers at low values. A cut is applied at 0.05 to remove these accidental triggers.

A continuing thread of the event selection deals with understanding and removing events caused by detector noise triggering in the DeepCore fiducial volume. While the rate of these accidental triggers is low at this stage relative to the rate at L3, they form an important background to the remaining set of neutrino events. In order to limit their effect, various cuts were investigated for the potential to separate signal neutrinos from the accidental background.

The most promising cut was discovered to be a remnant of earlier AMANDA processing efforts at separating atmospheric muon background and cascade signal events. This cut, called **Fill-Ratio**, looks at the topology and compactness of hits within an event.

Fill-Ratio requires a reconstructed vertex and pulse series. In the case of the GRECO L6, the first hit position in DeepCore within a 7.5 microsecond STW cleaned pulse series is used as an approximate event vertex. The hit series chosen, TWSRTOfflinePulses, offers some cleaning as well.

Once a vertex and pulse series are provided, a radius is computed. Many options are available for the caclulation of different radii, although the most effective for this event selection is the mean distance from the vertex.

$$\bar{r}_{Fill-Ratio} = A \left| \frac{\sum_i^{npulses} (\vec{x_i} - \vec{x}_{vertex})}{npulses} \right| \tag{7.3}$$

where A is a configurable scale factor. Within this radius, the algorithm indentifies all contained DOMs. The cut value is then given by the ratio of contained DOMs observing a pulse to the total number of contained DOMs.

$$f = \frac{\sum_i^{ncont} (|\vec{r_i}| < \bar{r}_{Fill-Ratio} \ \& \ Q_i > 0}{\sum_j^{ncont} (|\vec{r_j}| < \bar{r}_{Fill-Ratio}} \tag{7.4}$$

This effectively results in a measure of the compactness of a hypothetical cascade, where we expect the resulting hit distribution to be approximately spherically symmetric. In the case of an extended track, this parameter will yield a larger value of $\bar{r}_{Fill-Ratio}$. The larger value, in turn, will result in a higher number of contained DOMs and, therefore, a lower value of this parameter. This is particularly true in the case of accidental triggers, where we have no reason to expect a compact hit distribution a priori. Using a loose choice of A of 1.6, we concentrate the accidental triggers in just a few bins close to f=0.

The observed separation at a value of 0.05 allows up to one order of magnitude of reduction in the rate of accidental triggers with a relatively small reduction in signal rate of approximately 10%.

The L6 NChannel Cut

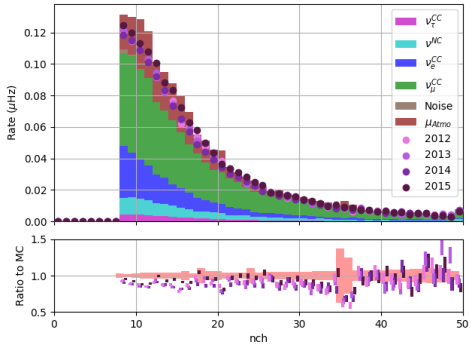

Figure 7.15 – The number of channels in a cleaned hit series. At least 8 hits are required for the reconstruction.

The reconstruction chosen for the final stages of this event selection attempt to reconstruct a total of eight variables: the position (x, y, z), time (t), the direction (θ, ϕ), the energy deposited in the proposed hadronic cascade (E_{casc}), and the track length (L). The reconstruction, described in more detail in 7.1.4, uses information both from the hit DOMs as well as unhit DOMs in order to constrain the reconstructed parameters. In order to constrain all parameters using observed hits, as opposed to relying on information from unhit DOMs, the decision was made to process only DOMs possessing more than 8 hits in the SRTTWOfflinePulsesDC pulse series.

In addition to providing a more robust reconstruction, the additional cut on the required number of hits further reduces the expected rate of accidental triggers in the detector by another order of magnitude. These accidental triggers make up about 0.3% of events in the sample following these cuts.

CorridorCut

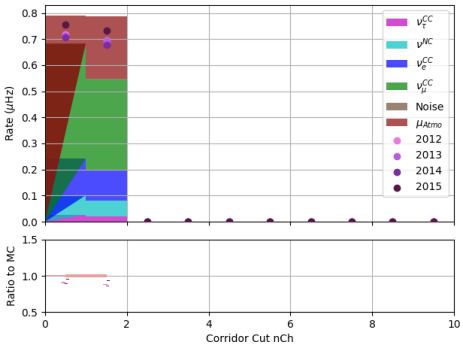

Figure 7.16 – The number of channels discovered along one of the various "corridors" in the detector. Events with at least two hits discovered along a corridor are removed.

At later cut levels, atmospheric muons continue to be problematic. Unfortunately muons at this level tend to be difficult to identify muons based on many parameters. Indeed, any muons that were easily identifiable have been removed already by this stage of the selection. In the past, minimum-ionizing muons were discovered to be leaking into the DeepCore fiducial volume along **corridors**, lines connecting the inner part of the detector to the outer edge without crossing any strings. These events pass between strings and leave little trace in the form of coincident hits in the outer detector.
In order to identify these muons, a cut was developed to look specifically along these pre-defined corridors for hits potentially correlated with pulses in DeepCore. Due to the effects of random detector noise, a cut limiting the number of discovered corridor hits to 0 would result in a significant loss of signal events. Instead, one hit is allowed, with two or more discovered DOMs leading to the removal of the event from further processing. At this stage, there are few events due to atmospheric muons with detectable energy in the veto, resulting in the removal of very few events.

FiniteReco Starting Containment

The SPE reconstruction used in L5 was created using an infinite muon hypothesis. In order to refine this reconstruction, the **FiniteReco** algorithm is employed.
FiniteReco is a module that accepts a previous reconstruction and a given set of pulses. The pulses are then used in a likelihood reconstruction in order to obtain estimates for the starting and stoppoing positions as well as the starting time for the given muon track. The direction of the muon track remains unchanged.
The starting position of the resulting reconstructed particle may be used to estimate the interaction point of the particle. **??** shows the position of the reconstructed vertex in terms of depth and distance from the center of the volume. If an event begins outside of the DeepCore fiducial volume, particularly if the event appears at the top of the fiducial volume, the event is likely to contain a muon and can be removed from the sample. Cuts are applied

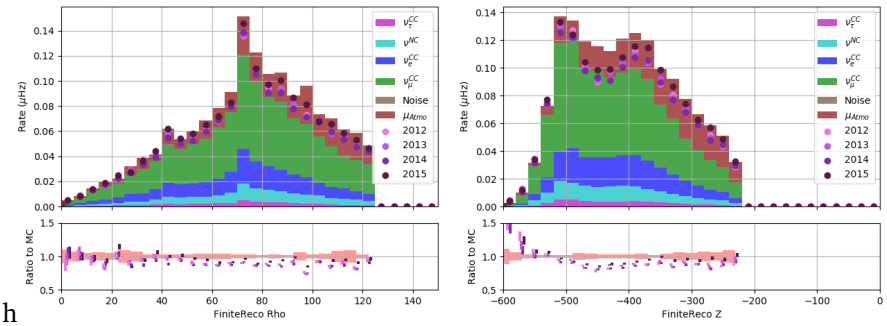

h

(a) $\rho_{FiniteReco}$ (b) $Z_{FiniteReco}$

Figure 7.17 – The FiniteReco containment cuts. Note the exces of muons at the top and outer edge of the DeepCore fiducial volume.

at the positions shown, resulting in a significant reduction in the number of muon events expected at final level.

7.1.4 GRECO Level 7: Final Level

Reconstruction using PegLeg

The existing reconstructions up to this point use either analytic or simplified likelihood reconstructions to estimate particle parameters. The position of the first hit and the finite muon reconstruction from FiniteReco provide straightforward separation power between atmospheric muons and neutrino events, but are designed to be computationally inexpensive instead of precise. At final level, these estimates are refined using a novel reconstruction method developed specifically for low-energy and oscillation searches with DeepCore.

The **PegLeg** reconstruction, developed by Martin Leuermann based, in part, on earlier work by Matt Dunkmann, is a low-energy reconstruction that uses a hybrid cascade+muon hypothesis. The reconstruction returns a total of eight parameters: the position (x_R, y_R, z_R), time (t_R), direction (θ, ϕ), total energy (E_R) and track length (L_R). The algorithm requires both seeds for each of the particle parameters, a collection of hits over which to run, and a set of splines fit to an ice model.

For each particle hypothesis, the event is broken into steps in time based on the timing of the observed hits in the event. At each time step, the expected charge at each DOM is calculated based on the energy and position of the particle emission scaled using the ice model splines. The charge expectation is evaluated for all DOMs, regardless of whether a hit is observed or not. The total likelihood of the hypothesis is then the product of the likelihoods at each DOM.

Given the large dimensionality of the space, significant computational power is required for the fit. Various steps are used in order to reduce the resource requirements. Track lengths are limited to integer values that depend on parameters used to produce the spline tables. While this requirement is lifted in newer versions of the software, that change has not yet propagated to the current GRECO events. In addition, only DOMs within 150 meters of the current particle position are evaluated to find the expected charge. All other DOMs are assumed to have an expected charge consistent with noise rates.

Each event takes approximately 15 minutes on average to converge in the reconstruction. There also exists a significant tail to the reconstruction time, sometimes extending to multiple

hours for a single event. With a large expected sample of events, the reconstruction time is the most computationally intensive part of the event selection

Containment with PegLeg

With a more refined reconstruction, additional constraints on the containment of events are possible. Similar to the work done with FiniteReco at L6, the Z_R and ρ_R values are shown in **??**. Once again, events at the top of and near the edge of DeepCore are more likely to be muons. Removing these events results in a 75% reduction of the atmospheric muon background at a cost of approximately 10% of the overall neutrino rate.

Other Cuts at L7

In the course of further work on the event selection, a number of issues previously-unknown were discovered. The most important of these is the discovery of **flaring DOMs**, which occur when a DOM spontaneously emits light. Because the light is emitted from the DOM itself, these events are characterized by high light yield on a single DOM relative to the rest of the event. These events were first discovered with the GRECO sample and are under further investigation within the IceCube collaboration. Two DOMs are known to emit light in this way at a rate of approximately once per day. A third DOM is suspected to emit lower light levels, but at a much more frequent rate.
The two known DOMs are removed from the reconstruction pending further investigation. In addition, any event event with a single DOM observing more than 80% of the total charge is removed to remove events with this characteristic signature.

7.2 The Properties of the GRECO Event Selection

The completion of cuts yields the completed GRECO event selection. There are many ways to characterize the final event sample.
One of the most general methods is via the **effective area**, a theoretical construct designed to allow a generic flux to be propagated to the selection. The effective area is a representation of the approximate cross section of a theoretical ideal detector. By combining the effective area and an arbitrary flux, an event rate can be obtained.
The ratio of the effective area at generation level and at a later cut level gives the efficiency of the selection. Because the event selection efficiency can change as a function of energy and direction,
The GRECO effective area for each of the neutrino channels is shown in **??**.

7.2.1 Energy and Zenith Reach

A Search for Tau Neutrinos from Oscillations

8

8.1 Unitarity of the PMNS Matrix

8.2 Current Limits on Unitarity

8.3 Systematics Considerations

8.3.1 Oscillation Parameters

8.3.2 Flux Uncertainties

Atmospheric Muon Flux

Neutrino Flux

8.3.3 Propagation Uncertainties

8.3.4 Cross-section Uncertainties

Axial Masses

DIS Cross-sections

8.3.5 Detector Systematics

While the previous systematics have been concerned with global physics parameters, the remainder are dedicated to understanding the uncertainties associated with the IceCube detector itself, such as the properties of the PMTs and the ice. These parameters, collectively referred to as the **detector systematics**, do not have known analytic forms and may affect the rate of events, the reconstruction properties of a given event, or both. The effect of these uncertainties must be evaluated using additional Monte Carlo simulations.

The GRECO event selection uses a number of simulation sets, shown in 8.1 for signal and 8.2 for background, to characterize the effects of these detector systematics. Each set contains at least one simulation parameter changed from the baseline set and are run through the full GRECO processing.

Set Number	Coincident Fraction	DOM Eff	Hole Ice	Forward Coeff	Absorption	Scattering	Livetime
Baseline	0%	100%	25	0	100%	100%	30 years
640C	100%	100%	25	0	100%	100%	30 years
641	0%	88%	25	0	100%	100%	30 years
643		94%					
644		97%					10 years
645		103%					5 years
646		106%					10 years
648		112%					
660	0%	100%	15	0	100%	100%	10 years
661			20				
662			30				
663			35				
670	0%	100%	25	2.0	100%	100%	10 years
671				-5.0			
672				-3.0			
673				1.0			
674				-1.0			
681	0%	100%	25	0.0	92.9%	92.9%	30 years
682					110%	100%	
683					100%	110%	

Table 8.1 – Systematics sets used for the characterization of the signal neutrino events. While all listed sets have up to 30 years of effective livetime available, not all events are processed in each set.

Set Number	Oversizing	DOM Eff	Hole Ice	Forward Coeff	Absorption	Scattering	Livetime	Comments
Baseline	1.0	99%	25	0	100%	100%	4 years	1 year standard + 3 years KDE filtered
A	1.0	69.3%	30	0	100%	100%	1 year	1 year standard
B		79.2%						
C		79.2%	25				3 years	3 years KDE filtered
D		89.1%						
E	1.0	99%	15	0	100%	100%	4 years	1 year standard + 3 years KDE filtered
F			30					
G	1.0	99%	30	-2	100%	100%	4 years	1 year standard + 3 years KDE filtered
H				-4				
I	3.0	99%	25	0	100%	100%	1 year	1 year KDE Filtered
J					110%			
K					80%			
L					100%	80%		
M						110%		
N						120%		
O					92.9%	92.9%		
P					114.2%	114.2%		

Table 8.2 – Systematics sets used for the characterization of the atmospheric muon background.

Coincident Fraction

The GENIE simulation sets are produced with exactly one neutrino interaction per event. In the actual detector, a fraction of triggered events will consist of a temporally coincident muon and neutrino pair which may be from the same air shower or from indepdent showers. In order to account for this possibility, a sample of such events are simulated assuming independent showers. In this case, every produced event contains at least one atmospheric muon in addition to exactly one neutrino interaction. By interpolating between this "100% coincident" sample and the standard "0% coincdent" sets, the effect of these events may be included in the final analysis.

The GRECO event selection actively selects against atmospheric muon-like events. The lowest-order effect of this choice is that increasing the coincident event fraction leads to a correspondingly lower total event rate, as shown in **??**. In order to distinguish the effect of the coincident events from a global normalization factor, the coincident event fraction is treated in a manner such that the total rate of events remains unchanged. The effect of this systematic in the final analysis is therefore shown in instead.

coin fraction figure

In most analyses in IceCube, a coincident event fraction of approximately 10% is assumed. This is derived from a combination of the atmospheric neutrino and muon fluxes assuming independent poissonian rates. At final level, the true fraction of coincident events is unknown, but previous oscillation analyses have found no clear issues using the standard simulation sets assuming no coincident events. A generous prior is therefore assumed to be a one-sided Gaussian distribution centered at 0% with a 10% width.

DOM Efficiency

As with all PMTs, the light detection probability of the IceCube DOMs is not perfect. Indeed, the total efficiency of detecting incident photons as measured by Hammamatsu, shown in **??**, is about 30% for the R7081-02 PMT used in standard IceCube DOMs. Before and during deployment, the net quantum efficiency of some DOMs were tested . The efficiency of the DOMs was again measured in-situo in order to better account for local effects like cable shadowing and the glass-ice interface. Dedicated measurement spost-deployment have used minimum ionizing muons in data and simulation and derived a modification of the assumed efficiency, hereafter referred to as the **DOM efficiency**, of 99%±10%.

Hammamatsu quantum efficiency? `http://www.hamamatsu.com/resources/pdf/etd/LARGE_AREA_PMT_TPMH1286E.pdf`

How many were tested in a lab before deployment?

Where does the domeff prior come from?

The DOM efficiency scales the probability of observing photons incident at the face of the DOM. A higher DOM efficiency leads to more information about individual particle interactions, leading to better reconstructions. The improved reconstructions lead to higher neutrino event rates at final level as well as more well-defined oscillation features in the reconstructed space. In addition, higher DOM efficiency increases the number of hits observed along atmospheric muon tracks, yielding improved veto efficiency. The net effect of changing the DOM efficiency by 10% is shown in .

domeff

Bulk Absorption and Scattering

The ice model used in IceCube is fit in-situo using various data from the deployment and detector operation in a process similar to the one described in 5.3. The model, here referred to as the **bulk ice model**, consists of scattering and absorption coefficients fit as a function of depth within the detector as well as information about anisotropy in the scattering properties of the ice . Uncertainties for these scattering and absorption coefficients, shown in , provide a significant source of uncertainty for physics measurements

ice model

bulk ice uncertainties vs depth

in IceCube. To handle these effects, global scale factors are used to modify all scattering or absorption coefficients in the bulk ice model simultaneously. Using the most recent published uncertainties on our ice model, a total uncertainty of approximately 10% is assumed for these global scale factors. Three variations are typically used, corresponding to sets with 10% larger absorption coefficients, 10% larger scattering coefficients, and a 7.1% reduction to both sets of coefficients.

The scattering and absorption exhibit different behaviors at final level in the GRECO sample. In general, the absorption behaves in a similar manner to the DOM efficiency, as both parameters modify the number of observed photons at the face of the PMT. In the signal samples, the effects of absorption uncertainties is relatively small. The most notable feature is an overall rate decrease (increase) for larger (smaller) absorption coefficients. As in the DOM efficiency, the depth of the oscillation minimum is also affected by the absorption coefficients due to a change in the reconstruction resolution.

The absorption, shown in , affects the atmospheric muons much more strongly than the neutrinos. Once again, this is due to the event selection: with weaker absorption (ie, smaller coefficients), more photons from the muon track may be detected. The observation of additional photons from the muon track improves the veto efficiency, leading to a significant decrease in the number of muons at final level.

absorption

The scattering, in contrast, has very little effect on the muon distribution, as seen in . No changes in rate or in reconstruction resolution are observed in the muon distributions.

scattering

In the neutrinos, the effects of the scattering are more important. In particular, stronger scattering (larger coefficients) lead to a reconstruction bias, with more events reconstructing as downgoing. This is a known effect of the reconstruction, where we use a version of the ice model which interprets off-time hits as being due to backscattered photons in a downgoing event.

Hole Ice and Foward Scattering

While the bulk ice refers to the scattering and absorption properties of the entire interaction volume, additional care must be taken for the ice close to the face of a PMT. During deployment, contaminants, including air, were introduced into the drill holes. These contaminants have been seen to form a dense column with unique scattering properties near the center of the drill holes. This bubble column, known as the **hole ice**, has properties separate from the rest of the ice model.

The uncertainties associated with the hole ice are significant and tend to elicit more attention than bulk ice uncertainties in searches for oscillations with DeepCore. The simulation of the hole ice model used here, discussed briefly in 4.2.4, requires two free parameters which will be referred to as the **lateral** and **forward** scattering parameters here for clarity. The lateral scattering modifies the efficiency of accepting photons incident from the horizon at each DOM while the forward scattering modifies only the acceptance of the very-forward region. The models of the angular acceptance are shown in .

hole ice and hifwd

The effects of the two hole ice parameters show very similar behavior to that of the scattering uncertainty in the bulk ice, as all three coefficients are modeling the scattering properties of different locations in the ice.

Parametrizing with Hyperplanes

For each of the simulation sets and each particle type, histograms are produced using the reconstructed energy, zenith, and track length. These systematic histograms give information about the expected change of the final histogram as a function of the changing systematics parameters, but the information is encoded in discretized points with statistical fluctuations due to the finite simulation statistics. In order to produce continuous systematics for analysis, the discrete detector systematics must be parametrized.

how do i flesh this out?

For this work, a hyperplane is fit to the detector systematics sets for each particle type and for each bin in the analysis histogram.

For neutrinos, a simple linear model is assumed for each detector systematic, with one free coefficient associated with each systematic as well as one free constant term independent of the systematics. The form of the hyperplane for each neutrino type in the bin ijk is given by 8.1.

$$f'_{ijk} = \left(\sum_{m}^{detsys} \left(a_m^{ijk} (x_m - x_m^0) \right) + b^{ijk} \right) f_{ijk} \tag{8.1}$$

muongun rates vs domeff and absorption to justify exponentials

For atmospheric muons, the form is slightly modified due to the strong effects observed from both the DOM efficiency and the absorption. In these two cases, an exponential model is selected to better describe the observed effects in simulation.

$$f_{ijk}\prime = \left(\sum_{m \neq DE,Abs}^{detsys} \left(a_m^{ijk} (x_m - x_m^0) \right) + \sum_{m}^{DE,Abs} \left(a_m^{ijk} e^{b^{ijk}(x_m - x_m^0)} \right) + c^{ijk} \right) f_{ijk} \tag{8.2}$$

Need to include some discussion of th goodness of fit for these sets. Maybe a plot of the chi2 values for all of the sets?

8.4 The Method of Maximum Likelihood

chi2 values for hyperplane parametrizations

8.4.1 The χ^2 Fit

The simplest implementation of a fitting algorithm begins with an assumption of the true and observed distributions. Namely, that the observed number of events in each bin of the histogram is drawn from a distribution approximately Gaussian with a mean μ equal to the expectation from simulations and a variance σ^2 calculated from the Poisson uncertainty on the expectation.

$$P\left(x|\mu\right) = Ne^{\frac{1}{2}\frac{(x-\mu)^2}{\sigma^2}} \tag{8.3}$$

where N is a normalization constant and, in the case of Poissonian statistics of simple histograms, the variance is given by the event weights in the specified bin.

$$\sigma^2 = \mu = \sum w \tag{8.4}$$

This needs work. can't even be called a derivation. its just crap.

From this point, taking the logrithm yields the standard χ^2 definition for the likelihood after dropping the constant terms.

$$\chi^2 = \frac{\left(x-\mu\right)^2}{\mu} \tag{8.5}$$

8.4.2 Finite Statistics

The χ^2 distribution above implicitly assumes that the dominant source of uncertainty at the best-fit point comes from the statistical fluctuations of the data around the true distribution represented by the Monte Carlo simulation. While this is true in te ideal case, in practice the statistical properties of the simulation sets themselves cannot be ignored. In general, every attempt should be made to ensure the statistical fluctuations of the simulation sets are negligible compared to those of the data. This typically leads to requests for at least an order of magnitude larger simulation statistics than expected from the data itself. In the situation where this is infeasible, modifications to the likelihood space itself may be used to account for the additional uncertainties. For this analysis the statistical uncertainties of the underlying simulation sets are added to the weighted uncertainties in quadrature.

make a plot showing chi2 value as a function of mc stats scale factor to justify the 10x rule

$$\chi^2_1 = \frac{1}{2}\frac{\left(x - \sum w\right)^2}{\left(\sum w\right)^2 + \sum w^2} \tag{8.6}$$

Due to the large uncertainties associated with the atmospheric muon sample, further considerations are necessary. In particular, the large uncertainties associated with atmospheric muon simulation statistics may be used by the fitter in order to reduce the χ^2_{FS} value. This situation proceeds with the minimization process as normal until a runaway effect is observed by increasing the statistical uncertainties at the expense of data/simulation agreement. In this case, the numerator becomes simply

$$\lim_{N_\mu \to \infty} \left(x - \sum w\right)^2 = \left(\sum w\right)^2 \tag{8.7}$$

The resulting limit in each bin as the event weights become large is therefore

$$\lim_{N_\mu \to \infty} \chi^2_1 = \frac{\left(\sum w\right)^2}{\left(\sum w\right)^2 + \sum w^2} \tag{8.8}$$

$$\lim_{N_\mu \to \infty} \chi^2_1 = 0 \tag{8.9}$$

While this is a particular concern for all simulation types, the dominant contribution to the $\sum w^2$ term is the atmospheric muons. In addition, the atmospheric muons have the strongest impacts from non-normalization systematic uncertaintines, particularly the DOM efficiency and the absorption. Modifying either of these parameters or the normalization systematics in the fit may lead to this runaway behavior.

In order to prevent this situation, a further modification of the χ^2 is necessary. For this analysis, the total scale of the statistical uncertainty is assumed to be set by the seed values of the fit.

$$N_{w^2} = \frac{\sum w^2_{Seed}}{\sum w^2} \tag{8.10}$$

With this modification, the χ^2 is now defined to be

$$\chi^2_{FS} = \frac{1}{2}\frac{\left(x - \sum w\right)^2}{\left(\sum w\right)^2 + N_{w^2}\sum w^2} \tag{8.11}$$

8.5 Parametrizing the Tau Neutrino Appearance

In order to properly measure the appearance of ν_τ events, a choise of "appearance parameter" must be selected. Here, we discuss the choice of parameter used in this analysis.

8.5.1 CC vs CC+NC

As described in 1.2, neutrinos may interact in two distinct ways to produce light in the IceCube detector. These two methods, the charged-current and neutral-current interactions, provide separate windows into neutrino interactions. Tau neutrino events may interact in either of these channels depending on the neutrino energy.

PDG

With a mass of 1776.82 ± 0.16 MeV and a lifetime of 290.3 ± 0.5 femtoseconds , τ leptons produced during neutrino oscillations in DeepCore tend to travel very short differences before decaying. The charged-current interactions of the ν_τ result in a variety of signatures due to the unique decay behavior of the τ lepton.

$$\tau^- \rightarrow \begin{cases} \mu^- \bar{\nu}_\mu \nu_\tau & 17.41 \pm 0.04\% \\ e^- \bar{\nu}_e \nu_\tau & 17.83 \pm 0.04\% \\ \text{Hadrons} & \text{Otherwise} \end{cases} \tag{8.12}$$

In either the muonic or the electronic decay modes, a fraction of the energy is lost to outgoing neutrinos, resulting in a smaller observed charge than would be associated with a corresponding interaction of another neutrino type. Furthermore, the muonic decay mode may lead to a visible muon track for the ν_τ interaction. These muon tracks associated with the appearance of ν_τ would appear at lower energies than the tracks corresponding to the ν_μ disappearance, allowing both effects to be observed simultaneously.

Unlike the varied results of the charged current interactions, neutral current interactions of neutrinos are assumed to have identical coupling and behavior, regardless of flavor and, therefore, undergo no observable change due to oscillations. Because of this, studies of the standard unitary PMNS matrix tend to treat neutral current events as effectively non-

superk paper, opera paper sources for un-oscillating NC

oscillating . In contrast, searches for new physics and sterile neutrinos result can result in a change in the apparent number of neutral current interactions in the detector.

For this analysis, both approaches have been adopted. A fit using charged-current events as the signal is used to provide limits on the modifications to a 3x3 mixing matrix without

non-sterile explanations of non-unitarity? maybe the neutrino decay paper?

the introduction of neutral-current altering behavior . A second fit, including both neutral current and charged current ν_τ events, provides more insight into possible extra flavors of neutrinos.

8.5.2 The ν_τ Normalization

Because effectively all ν_τ events observable in DeepCore are the result of neutrino oscillations, the total number of observed ν_τ interactions is a direct measure of the appearance itself. The number of ν_τ events interacting in DeepCore is, however, affected by many of the previously-discussed systematics. In particular, the number of events is strongly related to the assumed atmospheric oscillation parameters.

In order to provide a quantitative measure of the appearance, the overall normalization

think up a better phrasing to introduce the tau normalization

of signal events is used as a final physics parameter. The normalization is a fit parameter,

defined to be a total modification of the number of candidate ν_τ events after all other systematic parameters are applied.

$$f'_{ijk} = \sum_{m \neq \nu_\tau} f^m_{ijk}\left(\theta_{23}, \Delta m^2, ...\right) + N_{\nu_\tau} f^{\nu_\tau}_{ijk}\left(\theta_{23}, \Delta m^2, ...\right) \tag{8.13}$$

In this case, we end up with two general cases for the result. In the expected case, $N_{\nu_\tau} = 1.0$, we find that the number of candidate events is consistent with our modeling of the ν_τ and unitary PMNS mixing. If the value is significantly different from 1.0, we may have hints of either mismodeled cross-sections or of novel physics in the form of sterile neutrinos or neutrino mass state decay. Due to the large existing uncertainties in the PMNS matrix described in 8.1, either situation is likely to yield value information.

Crazy shit that I will probably take out. but maybe find the neutrino decay paper again?

8.5.3 Limits on the ν_τ Normalization

8.6 Expectations from Monte Carlo

8.6.1 Expected Contour

8.6.2 Expected Sensitivity over Time

8.6.3 Systematics Pulls

8.6.4 Feldman-Cousins vs WIlk's Theorem

8.7 Fitting Data

8.7.1 Burn Sample Fits: Testing the Fitting Code

8.7.2 Blind Fits: Checking the Goodness-of-Fit

8.8 Results from the Analysis

8.8.1 Individual Years

8.8.2 Combining Years of Data

8.8.3 Systematics Pulls in the Final Result

8.8.4 Implications and Future Work

9 Phase1: An Upgrade for Oscillation Searches

Notes